AD-A140 297 APPLICATION OF OPTICAL METHODS INCLUDING OPTICAL INTERFERENCE TO MEASURE T..(U) BRISTOL UNIV (ENGLAND) H H WILLS PHYSICS LAB K H ASHBEE ET AL. DEC 83 1/1

UNCLASSIFIED DAJA45-83-C-0030 F/G 11/9 NL

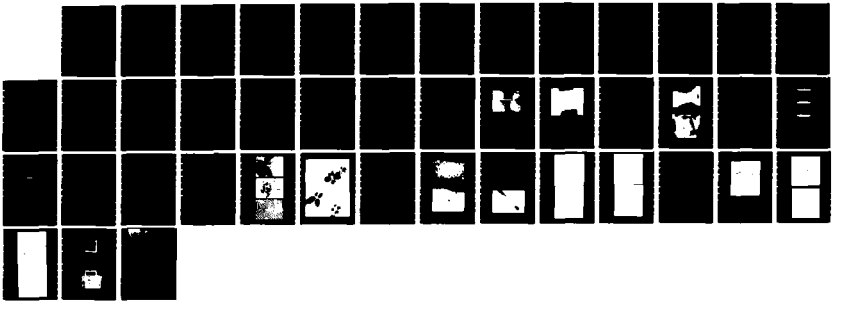

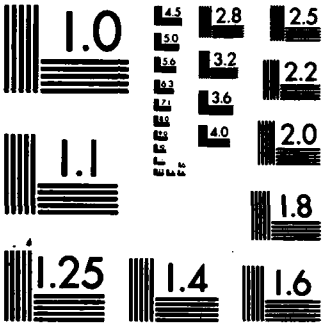

MICROCOPY RESOLUTION TEST CHART
NATIONAL BUREAU OF STANDARDS-1963-A

AD

APPLICATION OF OPTICAL METHODS, INCLUDING OPTICAL INTERFERENCE, TO MEASURE THE DIMENSIONAL STABILITY OF RESINS, RESIN BASED ADHESIVES AND RESIN BASED COMPOSITES

First Annual Progress Report

by

K H G Ashbee, Principal Investigator
J P Sargent

December 1983

United States Army

RESEARCH AND STANDARDIZATION GROUP (EUROPE)

London, England

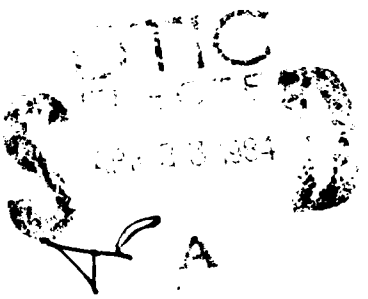

CONTRACT NUMBER DAJA45-83-C-0030

H H Wills Physics Laboratory, University of Bristol
Royal Fort, Tyndall Avenue
Bristol BS8 1TL, England

Key words

Polycarbonate, polyester, epoxy
Hairline cracks
Fracture toughness
Osmosis
Frost-shattering
Fracture mechanics
Optical caustics

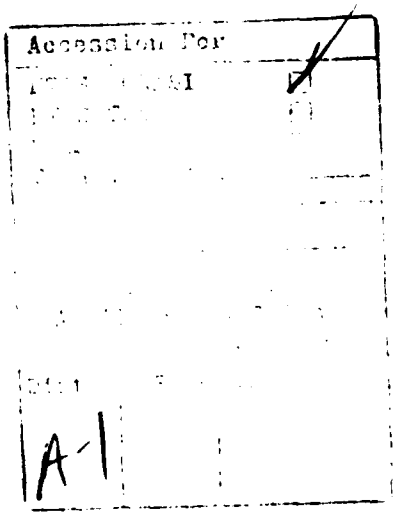

Abstract

As a consequence of osmosis during water uptake in the case of polycarbonates and as a consequence of osmosis followed by freezing of the aqueous solutions associated with osmosis in polyesters and epoxies, hairline cracks have been observed. The cracks are filled with water solution, and the small mismatch in acoustic impedance between polymer and water makes them extremely difficult to detect with ultrasound. Although the cracks are as much as a millimeter in lateral dimensions, the small separation between fracture surfaces and hence the small size of the crack volume makes for difficult detection by radiographic techniques. Specialised optical techniques, including rectified optics transmission microscopy and interferometry, appear to be the most satisfactory methods for their observation. These techniques have been used in the present studies and have permitted estimates to be made of the stress intensity factors at which hairline cracking occurs in each of the three polymers.

Direct evidence, in the form of photoelastic images around partially dissolved water soluble inclusions, and indirect evidence, in the form of the control effected by reducing the difference between the chemical potential of water in the solution around inclusions and that of water in the aqueous environment to which adhesive joints are exposed, is presented for concluding that a substantial part of the swelling is attributable to osmosis.

As light propagates through fibre reinforced transparent resins, it is common for focussing to occur. With perfect contact at the fibre/resin interface, focussing is possible only if the refractive index of the fibreglass exceeds that of the resin. In composites having identical refractive index for fibre and matrix materials, focussing occurs only if an interfacial gap has been created. The latter evidently affords a means for detecting and perhaps for estimating the nature (for example, air or water in the interfacial gap) and extent of interfacial debonding and has been investigated in some detail.

Introduction

There exists in the composite materials literature, very little by way of

failure analysis. This is because, unlike metal alloys, composites and more importantly, failures in composites, do not readily lend themselves to the identification of clear-cut microstructural variations that can be attributed to defects, to deficiencies in fabrication method, or to deficiencies in heat treatment (curing). It is with the need for better failure analysis uppermost in mind, that we have pushed to the limit our specialised optical methods for studying resin based materials. Specifically, we set out to investigate the lower limits of detection of separation between fibres and matrix during interfacial debonding in fibre reinforced resins.

Work done during the reporting period

(A) Hairline cracks in polycarbonates, polyester resins and epoxy resins.

The incorporation of solute within any polymer which behaves as a semi-permeable membrane will, during exposure of the polymer to solvent for that solute, lead to the formation of pockets of solution. The osmotic pressure associated with these pockets can be large enough to create internal fractures[1]. The present paper examines circumstances under which such pressure-filled cracks take the form of or lead to the formation of hairline cracks.

1 Osmotic pressure-filled cracks in polycarbonate

1mm thick specimens of a commercial polycarbonate (Makrolon) have been exposed to distilled water at 90C. Fig. 1 is an edge-on view of an osmotic pressure-filled crack photographed after 855 hours immersion. Fig. 2 shows a similar crack viewed face-on; the system of interference fringes generated within the cavity formed by the crack faces demonstrates that the crack opening displacement is nowhere greater than 10λ, where λ (546nm) is the wavelength of light used to take the photograph. A crack with this closeness between its faces we define as a hairline crack.

The interference fringes resolved in Fig. 2 permit accurate measurement of the crack opening displacement (COD) as a function of distance from the centre of the crack. This is plotted in Fig. 3 for various times of immersion and

reveals that the crack profile over most of its area does not approximate to either an elliptic shape (classical Griffith's theory) or to a parabolic shape (linear elastic fracture mechanics). In fact, approaching the crack edge there appears to be a definite inflection suggesting that the profile hereabouts is best represented by a cusp.

2 Polyester and epoxy resins

2.1 Deflated osmotic pressure-filled cracks

Osmosis also causes the creation of internal penny-shaped cracks in polyester resins and in epoxy resins. In these materials, the surfaces of osmotic pressure-filled cracks are relatively widely separated and the cracks can often be resolved by visual inspection. However, subsequent drying causes such cracks to deflate and take the form of hairline cracks, i.e. of cracks whose faces are separated by just a few wavelengths of light. Fig. 4a, b respectively show face-on views of cracks in 2 mm thick specimens of BXL Plastics PLC SR18979 polyester resin and in Ciba-Geigy PLC MY750 epoxy resin. Fig. 5 shows the crack profiles determined by counting fringes for deflated cracks in polyester and epoxy samples respectively. In both cases, the data can be fitted to parabolic relationships.

2.2 Frost-shattering

Another process whereby osmosis can lead to the occurence of hairline fractures in polyester and epoxy resins is lowering of the temperature of the pockets of solution in order to promote freezing.

Fig. 6 shows penny-shaped cracks seen edge-on in epoxy resin (a) after 168hrs immersion in distilled water at 90C, (b) after freezing and then thawing the solution contained within it and (c) after a second freeze/thaw cycle. It might be anticipated that the 8.4% volume expansion that accompanies the freezing of water would simply cause the existing crack to further propagate. However, this is not the case. Instead, a new crack is initiated, specifically an annular hairline crack beyond the edge of the existing lens-shaped crack. To aid the reader, the configuration in (c) of lens shaped crack

plus annular hairline crack is sketched in (d). Viewed face-on, the hairline crack is not detected, i.e. separation between its faces is too small to create even a single interference fringe.

The above phenomenon is akin to frost shattering in rocks. Fig. 7 is an example in a polyester resin. It does not occur in polycarbonates; in these materials osmotic pressure-filled cracks are already thin and, although freezing of the occluded solution may cause further extension of the existing crack, any additional separation between crack faces is insufficient to give rise to extra interference fringes.

3 Discussion

Other workers have used conventional fracture mechanics tests to measure the fracture toughness (K_{Ic}) of polycarbonates, polyester resins and epoxy resins. By general consensus, K_{Ic} lies between 2.2 and 3.2 $MPam^{1/2}$ for polycarbonates[3-6], between 0.41 and 0.84 for polyesters[7-10] and between 0.34 and 1.6 $MPam^{1/2}$ for epoxies[9,11-19].

Using values for Young's modulus (E) determined from ultrasonic measurements, i.e. ignoring any variation of E during time of crack growth, and assuming that hairline cracks are adequately described by linear elastic fracture mechanics and propagate at K_{Ic}, Eshelby's[20] equation (2.10) may be used to predict crack profiles

$$\Delta V = \frac{K_I \, r^{1/2}}{(2\pi)^{1/2}} \, 8 \, \frac{(1 - \mu^2)}{E} \qquad (1)$$

Here ΔV is the crack opening displacement and μ is the Poisson's ratio. This exercise has been carried out for each of the polymers studied here and gives rise to the curves drawn in Fig. 8. In each case, it is evident that far less crack opening displacement is observed in Fig. 3 and 5. than is predicted.

In polycarbonate the discrepancy between prediction and measurement cannot be

attributed to plasticity since additional strain resulting from permanent deformation (molecular orientation) at the crack tip would result in more crack opening displacement than is predicted by equation (1). Further, use of a more realistic value for E, in order to take into account the time dependence of modulus, would enhance the discrepancy. We are therefore forced to conclude that the values of K_I responsible for growth of the hairline cracks reported here for polycarbonates are considerably smaller than K_{Ic}.

In polyester and epoxy resins, hairline cracks of the deflated osmotic pressure-filled variety evidently do not grow with the geometries deduced from counting interference fringes. In a previous paper[2] the authors have applied equation (1) to measurements of inflated crack geometries in order to obtain values for K_I and have concluded that $K_I \sim K_{Ic}$ for fractures caused by osmosis in both kinds of resin.

The hairline cracks that constitute frost shattering are presumed to grow with crack opening displacements that are larger than those seen at room temperature. Taking as example, the epoxy shown in Fig. 4(a), the 8.4% volume expansion associated with freezing corresponds to a linear expansion of 2.8% so ΔV in eqn (1) is 2.8% of 14μm and r, the length to which the hairline crack extends, is approximately 4.6μm. Hence $K_I \sim 0.3$ MPam$^{1/2}$ which is at the lower end of the range of published values for K_{Ic}. A similar result is found for polyester samples. In both resins, hairline fracture is believed to occur rapidly. Although no audible click is heard when freezing takes place, subtraction of time for heat transfer ($\sim t^2/\alpha$ where t is the specimen half thickness and α is the thermal diffusivity) from the time required for hairline cracks to appear (of the order of seconds) indicates that hairline crack velocities could be of the order of 1 ms^{-1}.

To see how the fracture mechanics of hairline cracks in polyesters and epoxies compares with data for more slowly growing cracks in the same resins, the following analysis has been made of osmotic pressure-filled cracks. the velocities of osmotic pressure-filled cracks are typically $\sim 10^{-9}$ ms^{-1}[2], i.e. times of the order of days are required for growth to the dimensions shown in Fig 4. Hence the time dependence of Young's modulus needs to be taken into account when using equation (1) to estimate K_I. Assuming that they are elastic

cracks, we have used Westergaard's[21] equation (46) to obtain a value for Young's modulus which is more acceptable than the "instantaneous" value obtained ultrasonically.

$$2\eta_0 = \frac{4(1 - \mu^2)}{E} p \ (a^2 - x^2)^{1/2} \quad (2)$$

Where $2\eta_0$ is the crack opening displacement at distance x from the centre of a penny-shaped crack of radius a, μ is the Poisson's ratio and p is the traction applied to the surfaces of the crack. Data from Fig. 6,7 give values for E of 0.6 GNm^{-2} and 1.4 GNm^{-2} respectively for the epoxy and polyester samples that contain osmotic pressure-filled cracks.

Tables 1 and 2 respectively summarise the values for E and K_I obtained for the initial osmotic pressure-filled growth stage and for the frost cracking stage for both the epoxy and polyester samples.

Table 1. Growth under osmotic pressure

	crack velocity $ms^{-1} \times 10^{-10}$	E GPa	K_I $MPam^{1/2}$
epoxy	1.4	0.6	0.5
polyester	7.4	1.4	0.9

Table 2. Frost cracking

	crack velocity ms^{-1}	E GPa	K_I $MPam^{1/2}$
epoxy	1?	5	0.3
polyester	1?	5	0.3

(B) The contribution of osmosis to dimensional instability of adhesive joints (SERC supported work)

The application of a moiré technique to interference patterns generated between an optical flat and a thin adherend, during water uptake by model adhesive joints, has previously been used to detect and measure the swelling behaviour of proprietary adhesives[22,23]. Also previously reported[24] is the

mitigating effects on the rate of swelling and on the absolute magnitude of swelling at saturation, of inorganic salts in the aqueous environment to which joints are exposed. This latter observation appears to be indirect evidence for suspecting that osmotic pressure generation contributes to the swelling, and was attributed[24] to the possible presence of water soluble inclusions introduced as a consequence of the surface treatment applied to adherends.

1 Materials

In order to confirm or rule out the adherend as origin of water soluble inclusions which, when dissolved by diffused water, might generate sufficient osmotic pressure to influence the overall swelling, three different batches of model adhesive joints, conforming to the geometry reported in references 22 and 23, were fabricated. The first two employed a 150 μm thick soda-lime glass cover slip as flexible adherend and, respectively, soda-lime glass and aluminium pre-primed (The primer was a hot curing phenolic primer, identified as BR 1009/49) by Westland Helicopters Ltd as rigid adherend. (All glass components were first thoroughly cleaned by degreasing using a commerciall detergent, washing in distilled water, drying and then subjecting to ion-bombardment). The third batch of joints employed freshly cleaved 150μm and 500μm thick slabs of mica as flexible and rigid adherends respectively.

Two proprietary epoxy resin adhesive films were used to manufacture the joints. For reasons which will become evident, most of the joints were manufactured with Cyanamid FM 1000, a nylon modified epoxy film adhesive curing at 170C. The remainder were manufactured with Redux 312/5, a carrier supported nitrile rubber modified epoxy curing at 120 C.

All interference patterns were photographed during 60C immersion of the joint in either distilled water, or saturated KCl solution, or saturated NaCl solution.

2 Results

Circumferential moirè fringes, obtained by superimposition onto the initial undeformed interference pattern of the interference patterns re-photographed

during an immersion test, faithfully records the normal displacement[22]. Successive moirè fringes represent contours with $n\lambda/2$ normal displacement, where n is the fringe number and, may be used to determine the changing geometry of the cover slip. The innermost moirè fringe, representing the boundary between undisplaced cover slip and cover slip which has been displaced by $\lambda/2$ normal to the joint, migrates inwards as water uptake proceeds and can be used as a marker with which to determine the kinetics of swelling.

3 Experiments with different adherends

Figure 9 shows plots of the position of the first moirè fringe for various combinations of substrate and immersion medium. Figure 10 shows plots of the swelling profile, across half a diameter, for adhesive joints made from cover slip/FM 1000/glass and cover slip/FM 1000/aluminium, each immersed in distilled water and saturated NaCl solution respectively. It is evident that, within the limits of experimental uncertainty, both the swelling rate and magnitude of swelling at saturated water uptake are independent of the nature of the adherends, and are primarily functions of the immersion medium. Swelling is faster for joints immersed in distilled water than for identical joints immersed in salt solution. Also, the swelling at saturation is smaller for immersion in saturated salt solution than it is for immersion in distilled water. This behaviour is similar to that observed for cover slip/FM 1000/titanium joints[24].

It is evident from these findings that, for a given adhesive, the distribution and magnitude of the swelling that accompanies water uptake is independent of the choice of adherends. The swelling characteristics must therefore be attributed to the adhesive itself. It is also evident, from a comparison of the swelling behaviour for water uptake when immersed in distilled water and salt solutions that the adhesive behaves as a semi-permeable membrane. It is clear therefore, that the search for osmotic pressure filled pockets should be directed away from the adhesive/adherend interface and towards the adhesive itself.

4 Direct observation of pressure-filled cracks

Figure 11(a) shows a cover slip/FM 1000/glass joint after immersion for 48 hrs in distilled water at 60C. The regions of dark contrast are small undissolved inclusions contained within the adhesive. Under crossed polars the resin adjacent to each inclusion shows a characteristic pattern of stress birefringence, Figure 11(b). The pattern of the birefringence is consistent with there being a pressure associated with each inclusion. Accompanying any sizable concentration of inclusions is a marked local deformation of the cover slip. Figure 11(c), the interference pattern obtained from one such region, demonstrates this fact; the circular pattern of fringes indicates a small "hillock". Careful inspection of Figure 11(c) reveals that in the centre of the image there are discontinuities in the interference fringes where the local pressure must have been of sufficient magnitude (the tensile strength of glass is of the order of 2kbars) to burst the cover slip. Photoelastic evidence of pressure pockets was observed throughout this particular joint. Figure 12 shows an enlarged crossed polars image from a region which contains two inclusions.

Examination of an identical joint, after immersion in a saturated salt solution for 360 hrs at 60C, revealed a much lower incidence of pressure filled pockets. This is expected if osmosis attributable dissolution of water soluble material at the inclusions is responsible for the photo-elastic contrast; the pressure generated by osmosis is determined by the difference between the chemical potential of water in the solution at a particle and that in the aquoeus environment outside the joint, and this difference is smaller for saline environments than it is for pure water environments.

In order to check that the pressure pockets were not peculiar to this batch of adhesive (batch No. 4169), a second batch was aquired (batch No. 4307). Examination of a representative joint from this batch showed a similar, though slightly reduced, distribution of pressure pockets.

5 Experiments with a different adhesive

Figure 13 shows a plot of the swelling profile across a half diameter for a

cover slip/Redux 312-5/glass joint. Immersion in saturated NaCl solution has a mitigating effect upon the swelling, as was the case for FM 1000 joints, but no pressure filled pockets were observed.

(C) Caustics, shadows and fringes

As light propagates through fibre reinforced transparent resins, it is common for focussing to occur. In fibreglass composites designed for transmission of light, manufacturers try to match the refractive index of the resin with that of the fibreglass and in these materials focussing is realised only if an interfacial gap has been created, i.e. if debonding has occured. The focussed rays envelope a caustic surface, on the inside of which the intensity of light is enhanced and on the outside of which it is zero. That is , a bright-edged shadow is created and this shadow dominates the microscope image. Figure 14(a) shows an example for an E-glass/polyester resin composite which has experienced interfacial debonding as a consequence of 3 days immersion in boiling water. Figure 15(a) is a ray diagram reconstruction of the bright-edged shadow for a glassfibre embedded in resin and with a water solution filled gap at the interface. In a real composite the interfacial gap will, of course, be much smaller than that illustrated in Figure 15(a). Figure 15(b) shows the corresponding wavefront diagrams, computed using an optical path length of approximately 4λ between wavefronts with a nominal wavelength of 500nm. The consequences of reducing the gap size is to reduce the thickness of the shadows as demonstrated in Figure 16(a) and (b). It should be noted that in these diagrams no allowance has been made for multiple reflections from a single surface, nor for diffraction effects. In reality, diffraction phenomena will occur at any edge-like boundary.

If the interfacial gap is very small (less than $\lambda/2$), internal reflection is not total; a transmitted wave appears beyond the gap. Following Feynman[25], even though light is totally internally reflected from the resin/water solution interface, there are electric fields in the water solution which extend beyond the interface to a distance of the order of a wavelength, the amplitude of this "transmitted" wave dropping off exponentially with increasing distance from the interface, see Figure 17. Thus, if another interface is close enough, specifically the water solution/fibre interface in

our case, so that the "interfaces" in effect disappear, some light is transmitted.

Figure 16(a) and (b) respectively are the ray diagram and wavefront diagram for a gap of approximately $\lambda/2$, this being the minimum gap for which all light can be totally internally reflected. As the gap is further reduced, an increasing proportion of the light, nominally totally internally reflected, is transmitted. For light which is incident as shown in Figures 15 and 16, due account needs to be taken of the larger effective gap width for rays incident further away from than nearer to the fibre axis. Thus, although Figure 18 represents a gap width of $\lambda/20$, most of the light shown to be totally internally reflected is actually almost completely transmitted, save for a small region near the fibre edge, where the effective gap is indeed close to $\lambda/2$.

Figures 19 and 20 are ray and wavefront diagrams computed for a composite in which air has replaced water solution in the interfacial gap.

Close inspection of Figure 14(a) reveals the presence of a fringe around each fibre and this is more clearly resolved by making use of dark field illumination afforded by crossed polars, Figure 14(b). Except for the region of photoelastic contrast in the resin adjacent to it's end, a debonded fibre should not be detected when viewed between crossed polars; total extinction is expected for all rays of light passing through the fibre. However, as is evident from Figure 14(b), a region of bright contrast is seen at the fibre/resin interface. This is attributed to scattering from imperfections, including pits resulting from the etching action of caustic solution at the interface. Scattered light consists of rays with differently oriented planes of polarisation, their overall unpolarised nature may be demonstrated by viewing and rotating a ground glass screen mounted between crossed polars on a polariscope, see Figure 21. The fact that the fringe contrast around each fibre exists when polars are crossed suggests that they also have their origin in scattering. With the objective lens slightly far-focussed, i.e. focussed on a plane slightly beyond that containing the fibre axis, the number of fringes increases as illustrated in Figures 14(c) and (d).

Berry and Hajnal[26] have calculated the optical effects of simple non-planar interfaces between media of different refractive index. Specifically, they considered the surface deformations on water that are created at the edge of a floating razor blade and around a floating sphere. The razor edge gives rise to an illuminated region that is bounded by a caustic which imparts a bright-edged shadow, decorated with Airy-function fringes. The sphere gives an approximately paraboloidal caustic decorated with bright Airy-function fringes (produced by the curved air/water interface) within which are faint Bessel-function fringes (produced by the circular boundary at the surface of contact between sphere and water).

The fringe contrast around a fibre might reasonably be expected to consist of that due to diffraction by a straight edge plus, around its ends, something similar to that due to diffraction at the circular line defined by the water level in Berry and Hajnal's sphere experiment. The two sets of fringes would, of course, join together smoothly.

Plans for the remainder of the contract period

(A) Resins

Ciba-Geigy's recommended cure schedules for MY 750 epoxy resin are
4 hours at 100C + 1 hour at 130C + 3-6 hours 180C
An attempt will be made to use our moire optical interference technique to measure the dimensional changes that accompany each of several cure times in the above range of cure schedules.

(B) Adhesives

The moire optical interference technique will also be used to measure dimensional changes during water uptake by glass cover slip/3M adhesive/glass microscope slide joints.

(C) Composites

The newly discovered optical caustics phenomena reported in this first annual report will be further investigated as a potential method for failure analysis of real composites.

References

1. K.H.G. Ashbee F.C. Frank and R. Wyatt, Proc. Roy. Soc. A300, 415 (1967).
2. J.P. Sargent and K.H.G. Ashbee, J.Appl.Poly.Sci. in press (1983).
3. A.P. Glover, F.A. Johnson and J.C. Radon, Poly. Engng. Sci. 14, 420 (1974).
4. M. Parvin and J.G. Williams, J. Mat. Sci. 10, 1883 (1975).
5. R. Ravetti, W.W. Gerberich and T.E. Hutchinson, J. Mat. Sci. 10, 1441 (1975).
6. H. Uete and R.M. Coddell, Int. J. Mech. Sci. 25, 87 (1983).
7. M.J. Owen and R.G. Rose, J.Phys.D. 6, 42 (1973).
8. G. Pritchard, R.G. Rose and N. Taneja, J.Mat.Sci. 11, 718 (1976).
9. A.S. Kobayashi and S. Mall, Polymer Engng. and Sci. 19, 131 (1979).
10. S.J. Harris, J.M. Hutchinson and F. Nedjet-Hayem, PRI Conf. on Deformation and Fracture of Polymers, Cambridge 1982.
11. H.T. Corten in "Fundamental Aspects of Fibre Reinforced Composites", ed. R.T. Schwartz and H.S. Schwartz, Interscience, 1968, p.98.
12. S.C. Kunz and P.W.R. Beaumont, 4th PRI Conf., London 1976, paper 14.
13. W.T. Evans and B.I.G. Barr, J.Strain Anal. 9, 166 (1974).
14. H.T. Corten in "Reinforced Plastics" ed. E. Baer, Reinhold, 1964.
15. D.C. Phillips and J.M. Scott, J. Mat. Sci. 9, 1202 (1974).
16. A.C. Moloney, H.H. Kausch and H.R. Steiger, J.Mat. Sci. 18, 208 (1983).
17. E.J. Ripling, C. Bersch and S. Mostovoy, Adhesion 3, 145 (1971).
18. W.D. Bascom, Proc. Crit. Rev. on Composite Materials, US Army Materials and Mechanics Research Center, MS 82-3, 1981, p.415.
19. R.A. Gledhill, A.J. Kinloch, S. Yamini and R.J. Young, Polymer 19, 574 (1978).
20. J.D. Eshelby, Sci. Prog., 59, 161 (1971).
21. H.M. Westergaard, J. Appl. Mech., A49, (1939).
22. J. P. Sargent and K. H. G. Ashbee, J. Adhesion., 11, 175(1980).

23. D. E. Jesson and J. P. Sargent, J. Adhesion., 14, 119(1982).
24. J. P. Sargent and K. H. G. Ashbee, J. Phys. D., 14, 1933(1981).
25. R. P. Feynman, R. B. Leighton and M Sands, in "The Feynman Lectures on Physics" vol 2, Addison Wesley, 1965.
26 M. V. Berry and J. V. Hajnal, Optic Acta., 1 30(1983).

Figure Captions

Figure. 1 Osmotic pressure-filled crack in polycarbonate

Figure. 2 Same as Fig. 1 but viewed face-on

Figure. 3 COD across a half diameter for different immersion times

Figure. 4 Osmotic pressure-filled cracks after drying (a) epoxy (b) polyester[2]

Figure. 5 Profiles for deflated cracks[2]

Figure. 6 Osmotic pressure-filled crack in an epoxy specimen after (a) 168 hours immersion at 90C (b) one freeze/thaw cycle (c) two freeze/thaw cycles (d) Schematic of (c) with hairline crack indicated by an arrow

Figure. 7 Osmotic pressure-filled crack in polyester after one freeze/thaw cycle

Figure. 8 Predicted COD profiles (a) polycarbonate, K_{Ic} = 2.7MPam$^{1/2}$, E = 5GPa, (b) polyester, K_{Ic} = 0.6MPam$^{1/2}$, E = 5GPa, (c) epoxy, K_{Ic} = 1.0 MPam$^{1/2}$, E = 5GPa

Figure 9. Migration rate of the first moiré fringe plotted against time$^{1/2}$ for various combinations of adherends and immersion media. All at 60C.

- ○ cover slip/FM 1000/glass, distilled water
- ◐ mica/FM 1000/mica, distilled water
- ● cover slip/FM 1000/aluminium, distilled water
- ◻ cover slip/FM 1000/glass, saturated NaCl solution
- ◧ mica/FM 1000/mica, saturated NaCl solution
- ■ cover slip/FM 1000/aluminium, saturated NaCl solution
- ◆ mica/FM 1000/mica, saturated KCl solution

Figure 10. Radial distribution of displacement of the cover slip normal to FM 1000 joints after 48 hours immersion at 60C.

Upper curves —— cover slip/FM 1000/glass, distilled water

– – – cover slip/FM 1000/aluminium, distilled water

Lower curves —— cover slip/FM 1000/glass, saturated NaCl solution

– – – cover slip/FM 1000/aluminium, saturated NaCl solution

Figure 11a. Photomicrograph of a region of a cover slip/FM 1000/glass joint after immersion in distilled water for 40 hours at 60C

b. Same as (a) with crossed polars

c. Interference pattern revealing the normal displacement for the region shown in (a)

Figure 12. Photoelastic image of pressure pockets located within the adhesive after 48 hours immersion in distilled water at 60C.

Figure 13. Radial distribution of displacement of the cover slip normal to a Redux 312/5 joint after 120 hours immersion at 60C.

Upper curve; cover slip/Redux 312-5/glass, distilled water

Lower curve; cover slip/Redux 312-5/glass, saturated NaCl solution

Figure 14. An E-glass/polyester resin composite after 3 days immersion in boiling water. (a) Viewed with transmitted light. (b) Same as (a) but with polars crossed. The action of diffused water at the interface has destroyed the transfer of load arising from resin shrinkage, thereby rendering the fibres stress-free and therefore birefringence-free. (c) and (d) same as (a) and (b) respectively but at longer focus.

Figure 15a. Ray diagram reconstruction for a glass fibre embedded in resin with a water solution at the interface. Fibre diameter is 10μm. Interfacial gap is ∿ 1/2 a fibre diameter.

b. Same as (a) but showing the wavefronts. Wavefronts plotted at 4λ optical path length intervals.

Figure 16a. Ray diagram reconstruction for a glass fibre embedded in resin with a water solution at the interface. Fibre diameter is 10μm. Interfacial gap is λ/2.

b. Same as (a) but showing the wavefronts. Wavefronts plotted at 4λ optical path length intervals.

Figure 17. Graph showing the "transmitted" electric field amplitude as a function of distance from the interface following total internal reflection. After Feynman[25].

Figure 18. Ray diagram reconstruction for a glass fibre embedded in resin with a water solution gap of λ/20. Ignoring the consequences of the "transmitted flux".

Figure 19. Same as Fig. 15, but with an air gap.

Figure 20. Same as Fig. 16, but with an air gap.

Figure 21. Scattered light viewed between crossed polars.

Annex

With a reduced grant ($60,352 over two years compared with $62,861 over two years for DAJA-37-81-C-0214) and in a period of 5% inflation, we have been obliged to operate at a somewhat lower level of staffing than hitherto.

A polaroid land camera has been purchased for £414.

There are $0.00 of unused funds remaining on the contract at the end of the period covered by this report.

INVOICE

Request payment of $9,540.00 for the First Annual Progress Report covering the period January 1983 to December 1983 on Contract No DAJA-45-83-C-0030.

Report was submitted to the US Army European Research Office on December 16, 1983.

"I certify that the above bill is correct and just, that payment therefore has not been received, and that the prices therein are exclusive of all taxes".

M J Bishop

pp THE FINANCE OFFICER
UNIVERSITY OF BRISTOL

M J Bishop, Administrative Assistant

December 16, 1983.

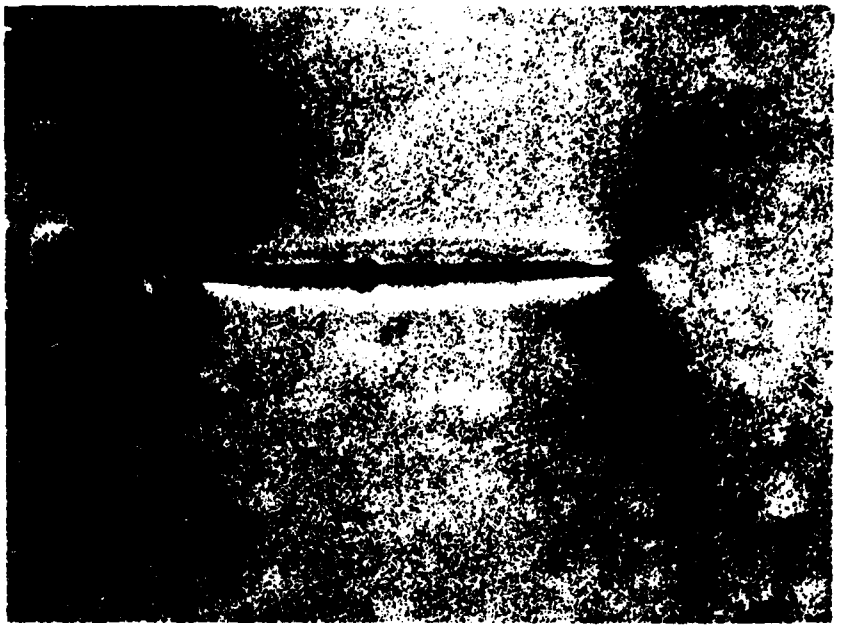

Figure. 1 Osmotic pressure-filled crack in polycarbonate

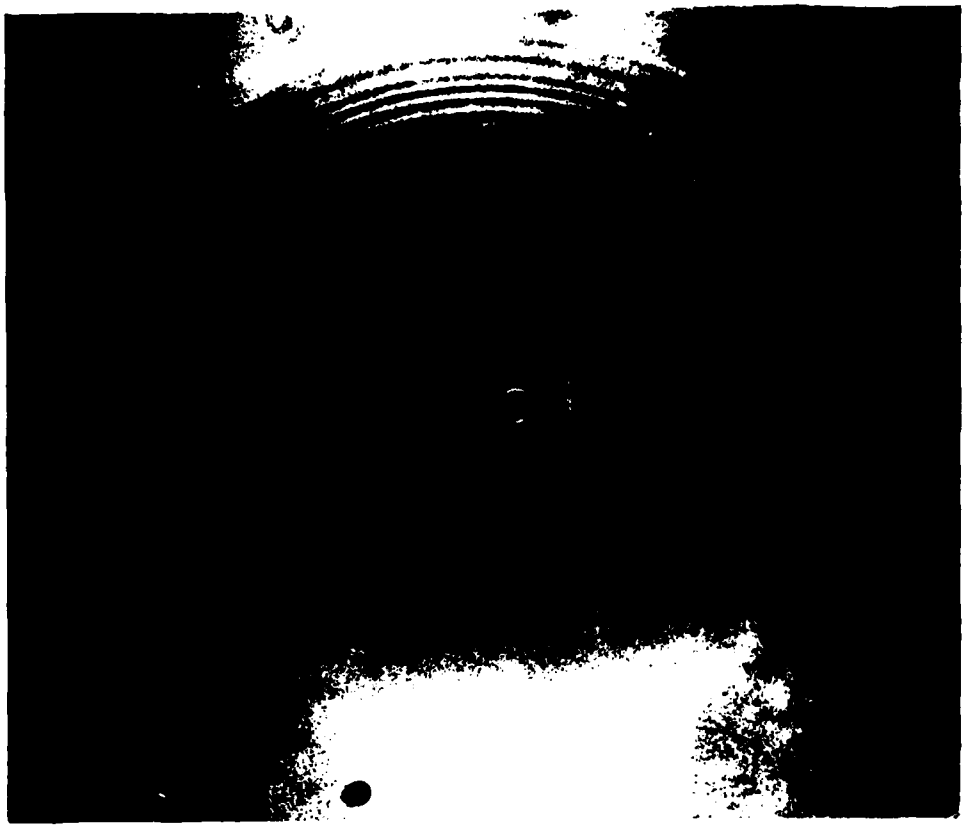

Figure. 2 Same as Fig. 1 but viewed face-on

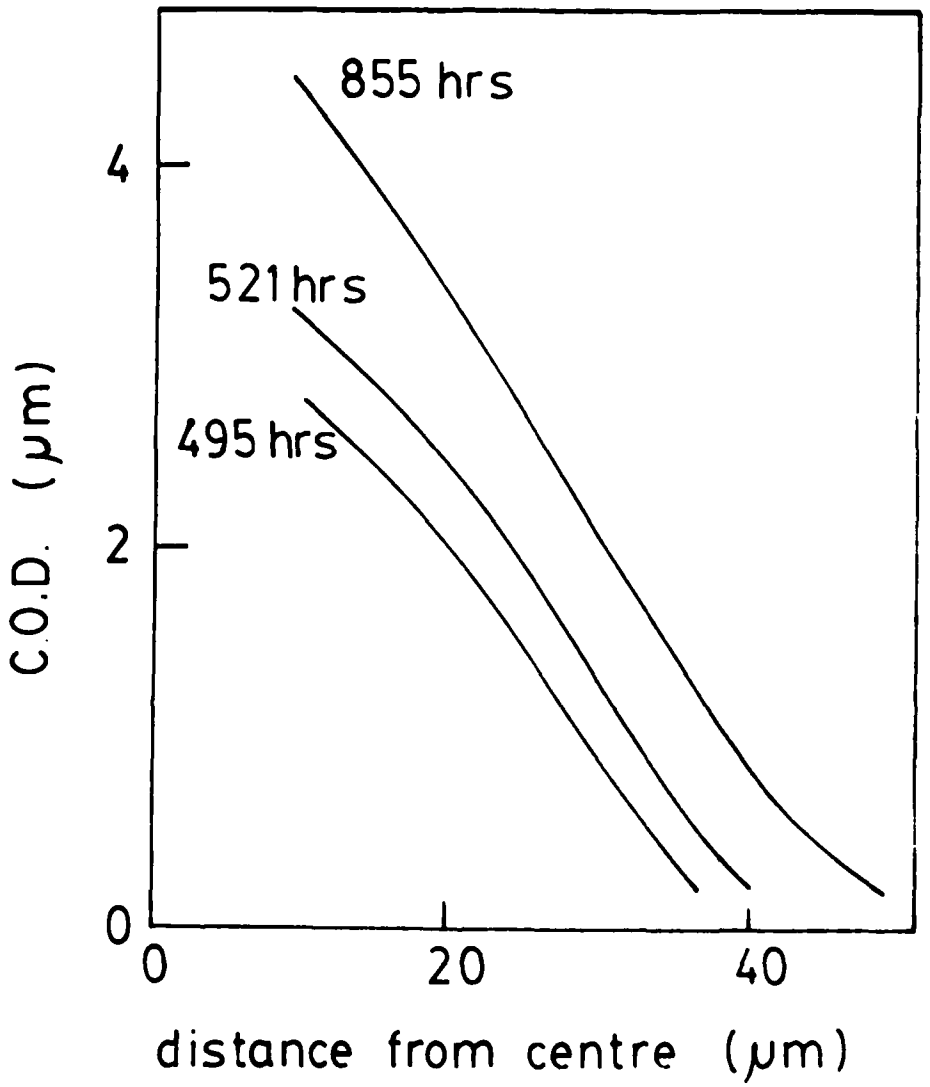

Figure. 3 COD across a half diameter for different immersion times

a

b

Figure. 4 Osmotic pressure-filled cracks after drying (a) epoxy (b) polyester[2]

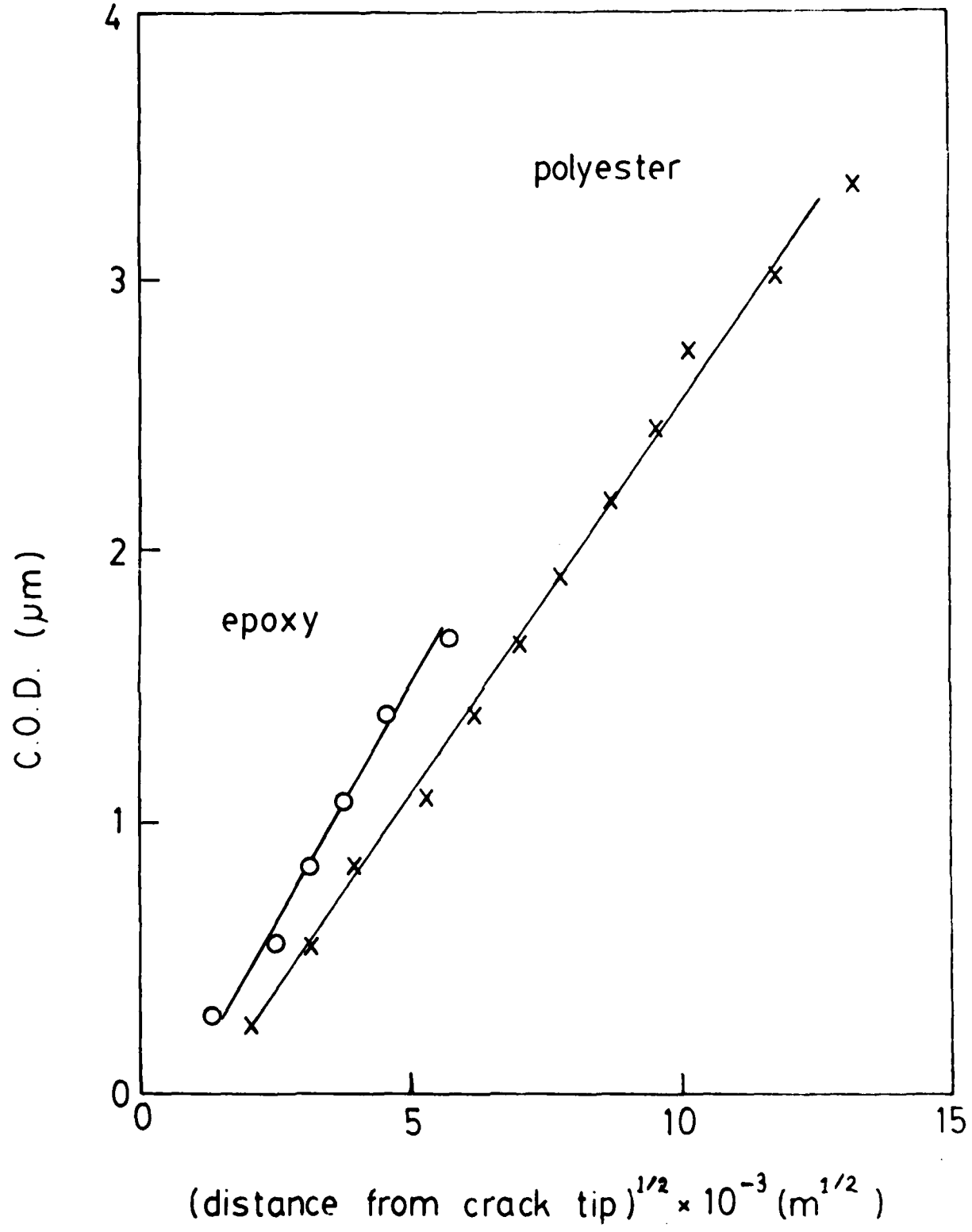

Figure. 5 Profiles for deflated cracks[2]

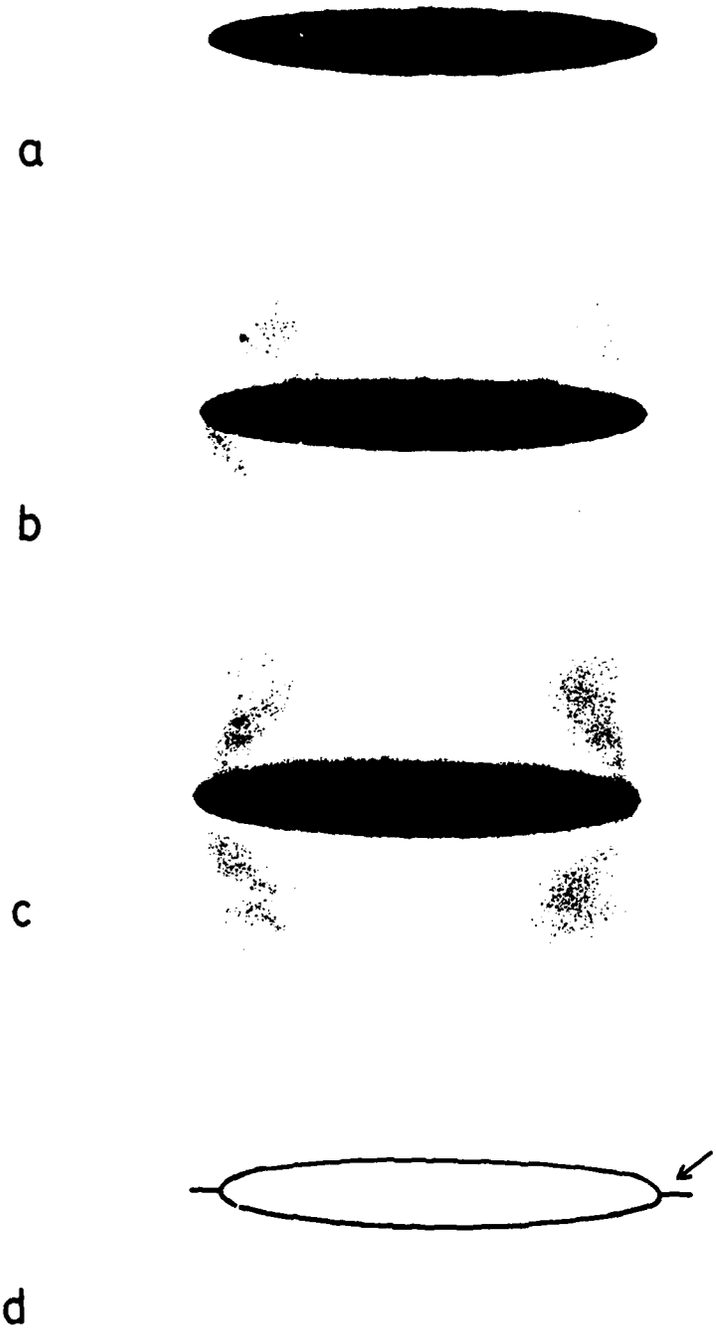

Figure. 6 Osmotic pressure-filled crack in an epoxy specimen after (a) 168 hours immersion at 90C (b) one freeze/thaw cycle (c) two freeze/thaw cycles (d) Schematic of (c) with hairline crack indicated by an arrow

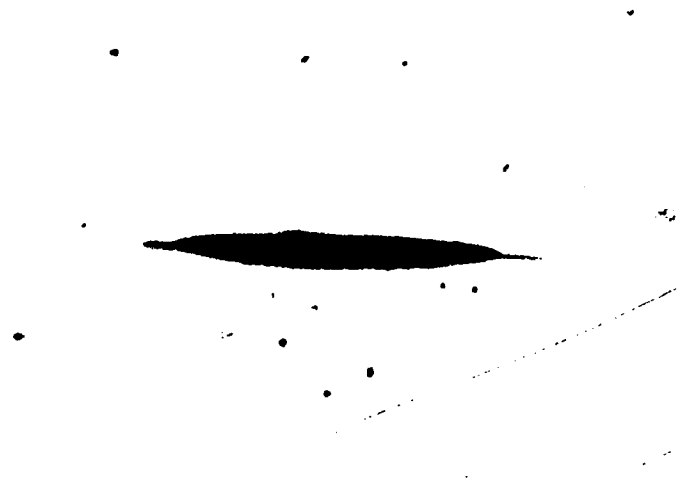

Figure. 7 Osmotic pressure-filled crack in polyester after one freeze/thaw cycle

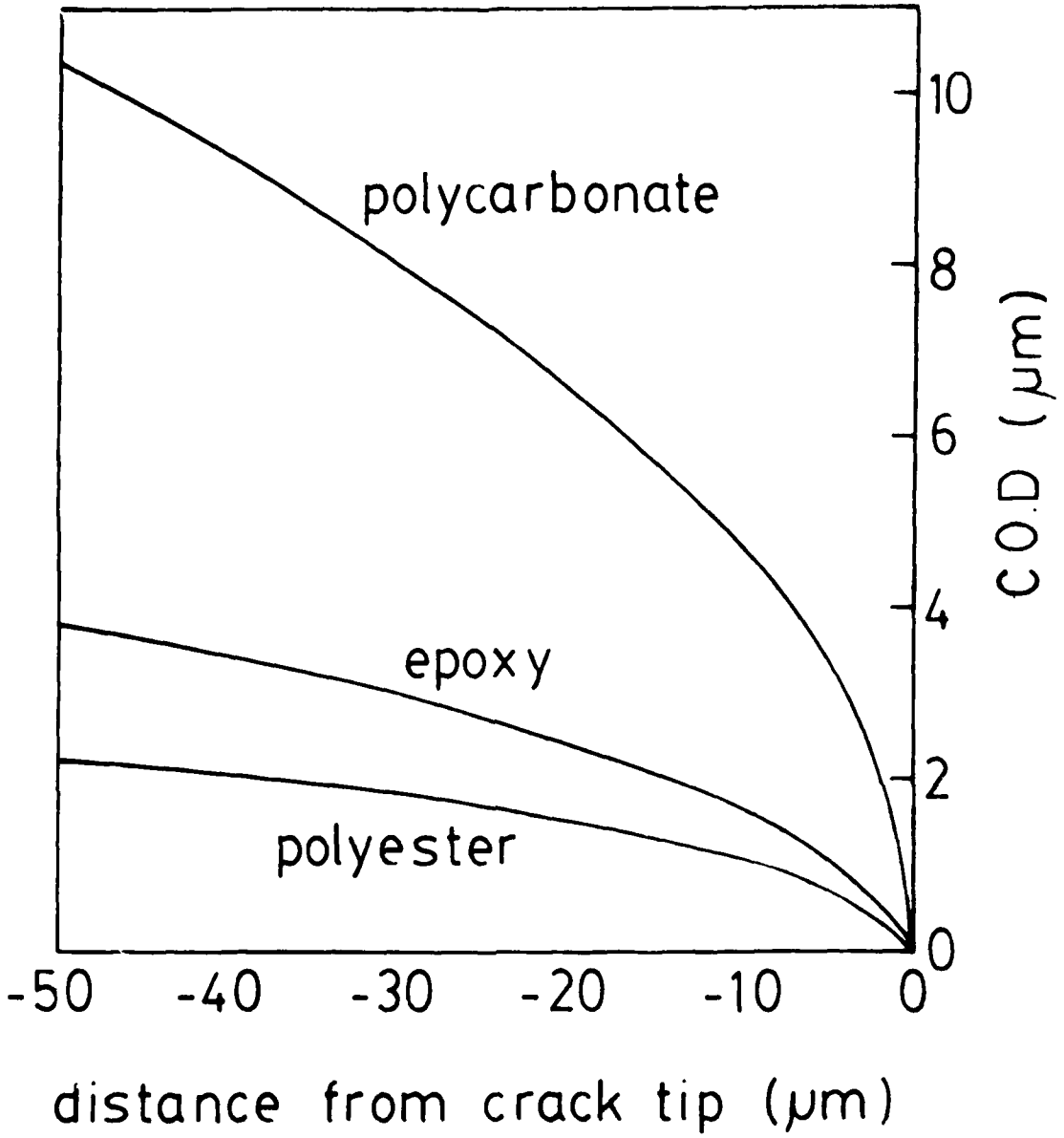

Figure. 8 Predicted COD profiles (a) polycarbonate, K_{Ic} = 2.7MPam$^{1/2}$, E = 5GPa, (b) polyester, K_{Ic} = 0.6MPam$^{1/2}$, E = 5GPa, (c) epoxy, K_{Ic} = 1.0 MPam$^{1/2}$, E = 5GPa

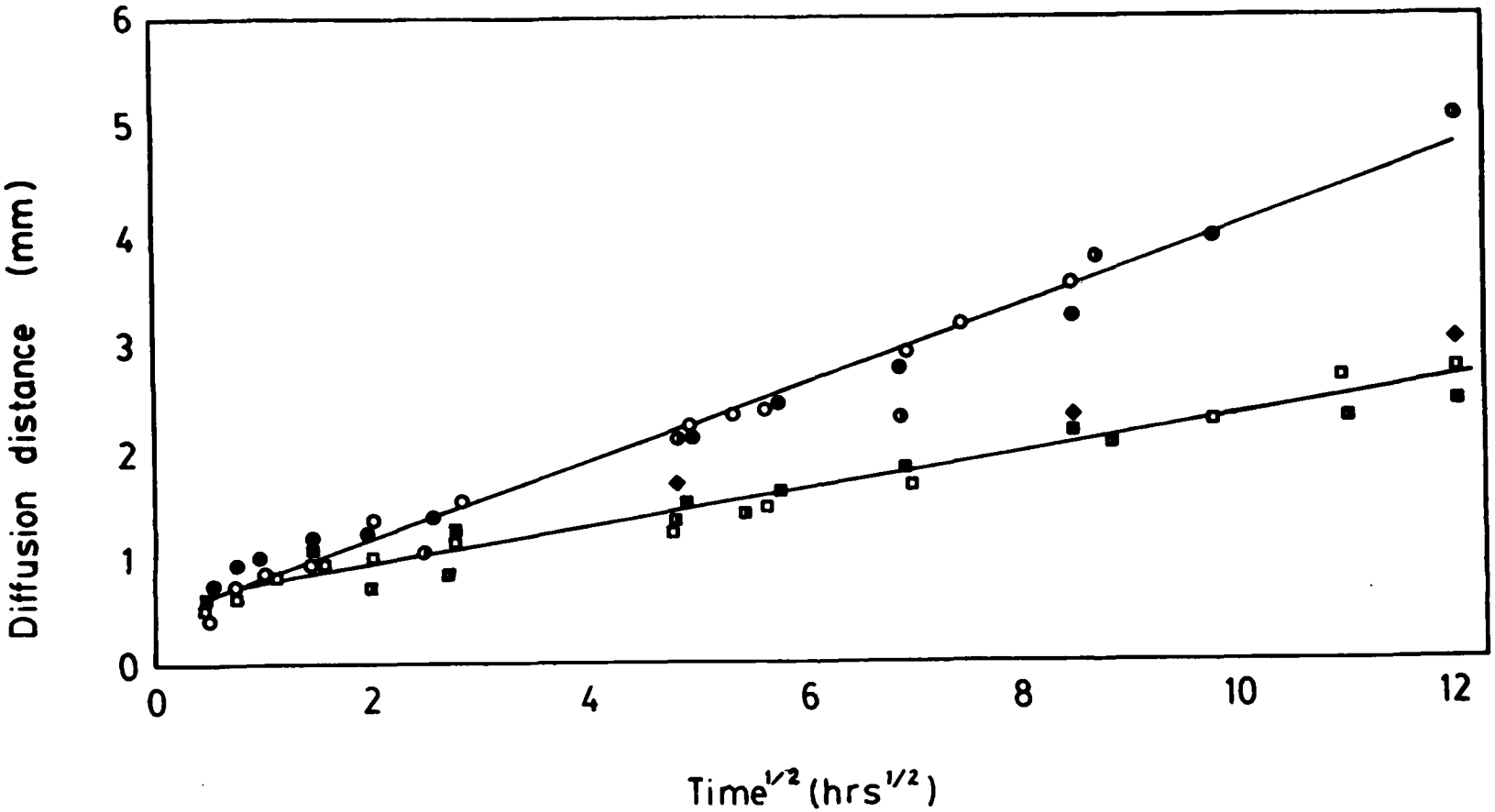

Figure 9. Migration rate of the first moiré fringe plotted against time$^{1/2}$ for various combinations of adherends and immersion media. All at 60C.

- ○ cover slip/FM 1000/glass, distilled water
- ◐ mica/FM 1000/mica, distilled water
- ● cover slip/FM 1000/aluminium, distilled water
- □ cover slip/FM 1000/glass, saturated NaCl solution
- ▮ mica/FM 1000/mica, saturated NaCl solution
- ▯ cover slip/FM 1000/aluminium, saturated NaCl solution
- ◆ mica/FM 1000/mica, saturated KCl solution

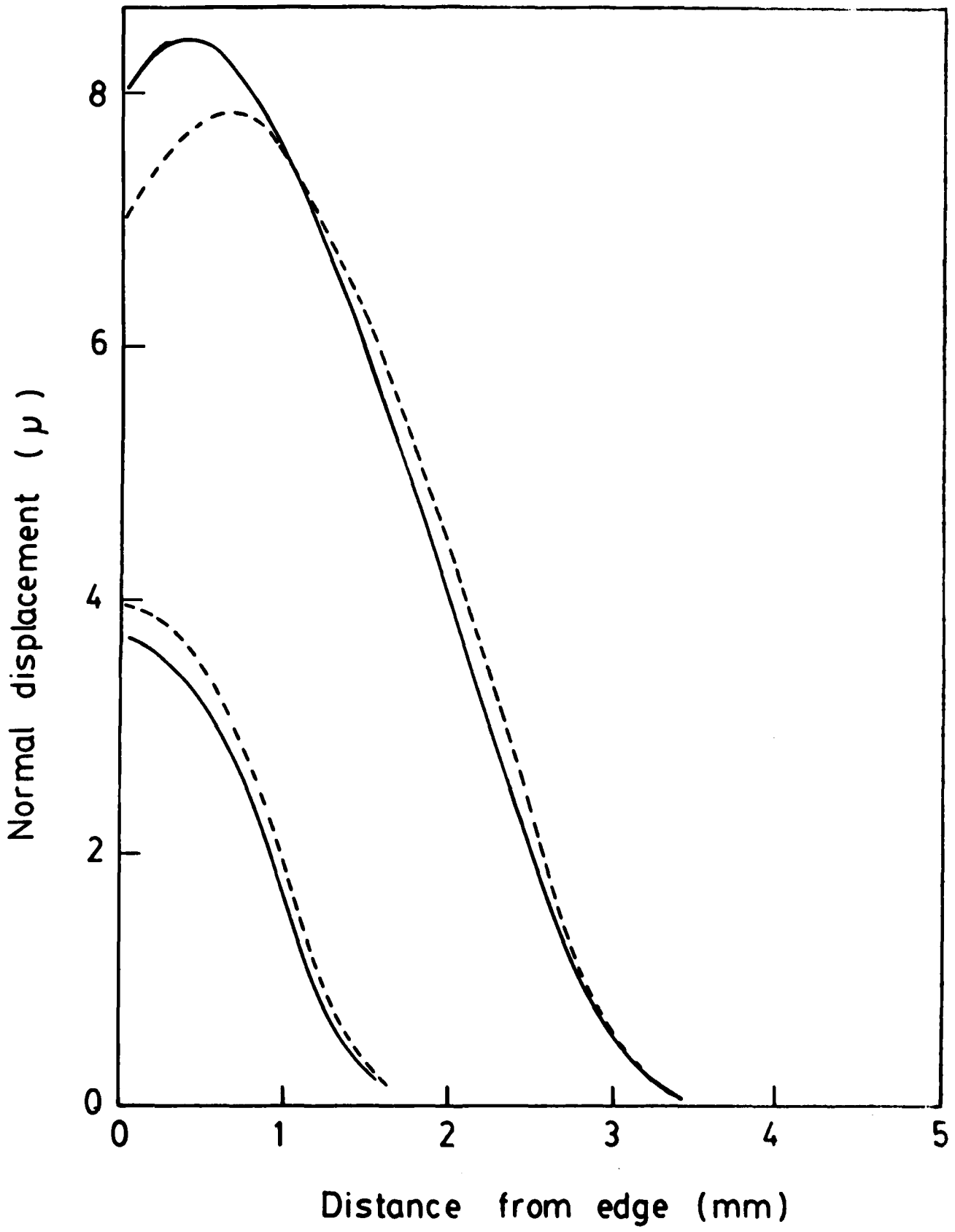

Figure 10. Radial distribution of displacement of the cover slip normal to FM 1000 joints after 48 hours immersion at 60C.

Upper curves —— cover slip/FM 1000/glass, distilled water

--- cover slip/FM 1000/aluminium, distilled water

Lower curves —— cover slip/FM 1000/glass, saturated NaCl solution

--- cover slip/FM 1000/aluminium, saturated NaCl

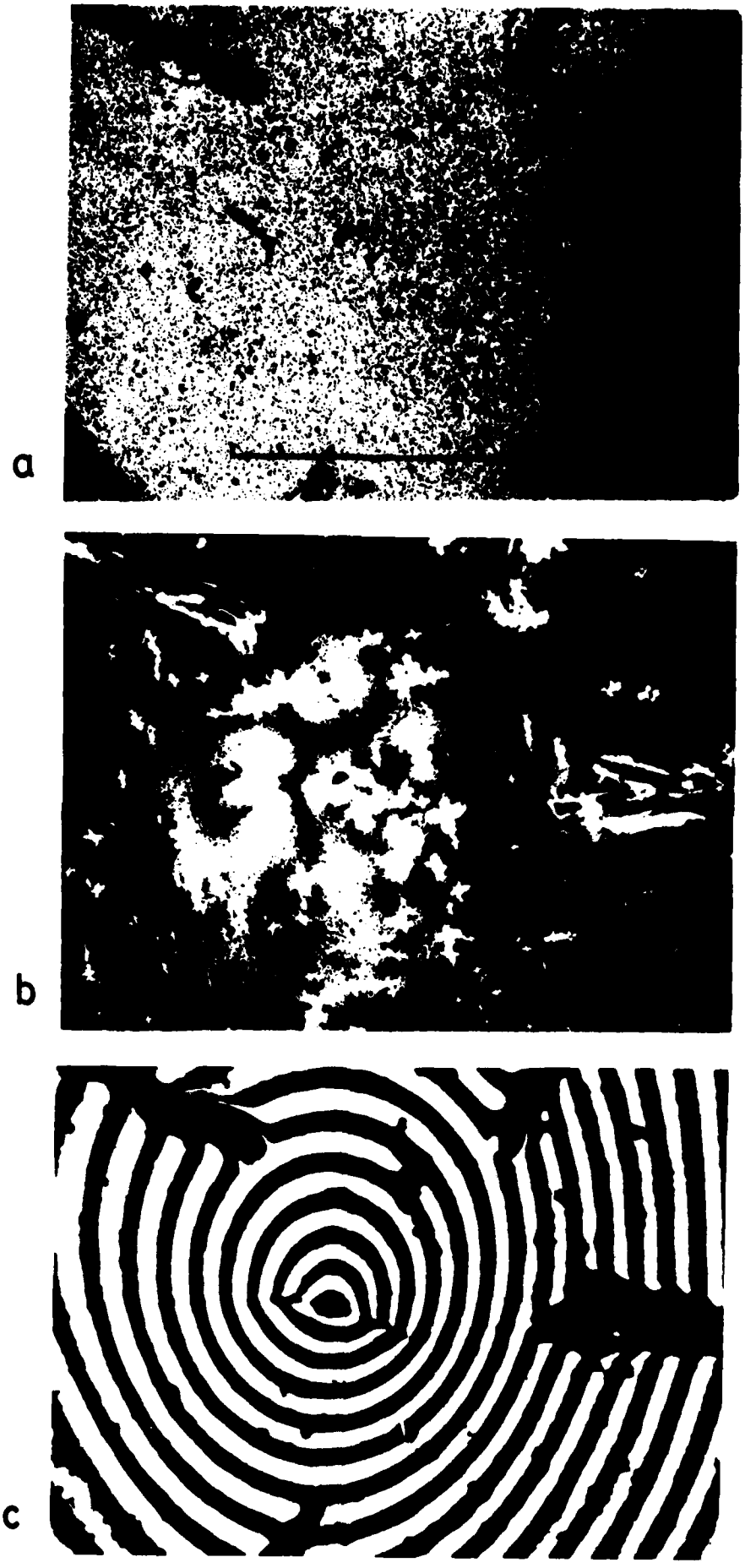

Figurella. Photomicrograph of a region of a cover slip/FM 1000/glass joint after immersion in distilled water for 40 hours at 60C
b. Same as (a) with crossed polars

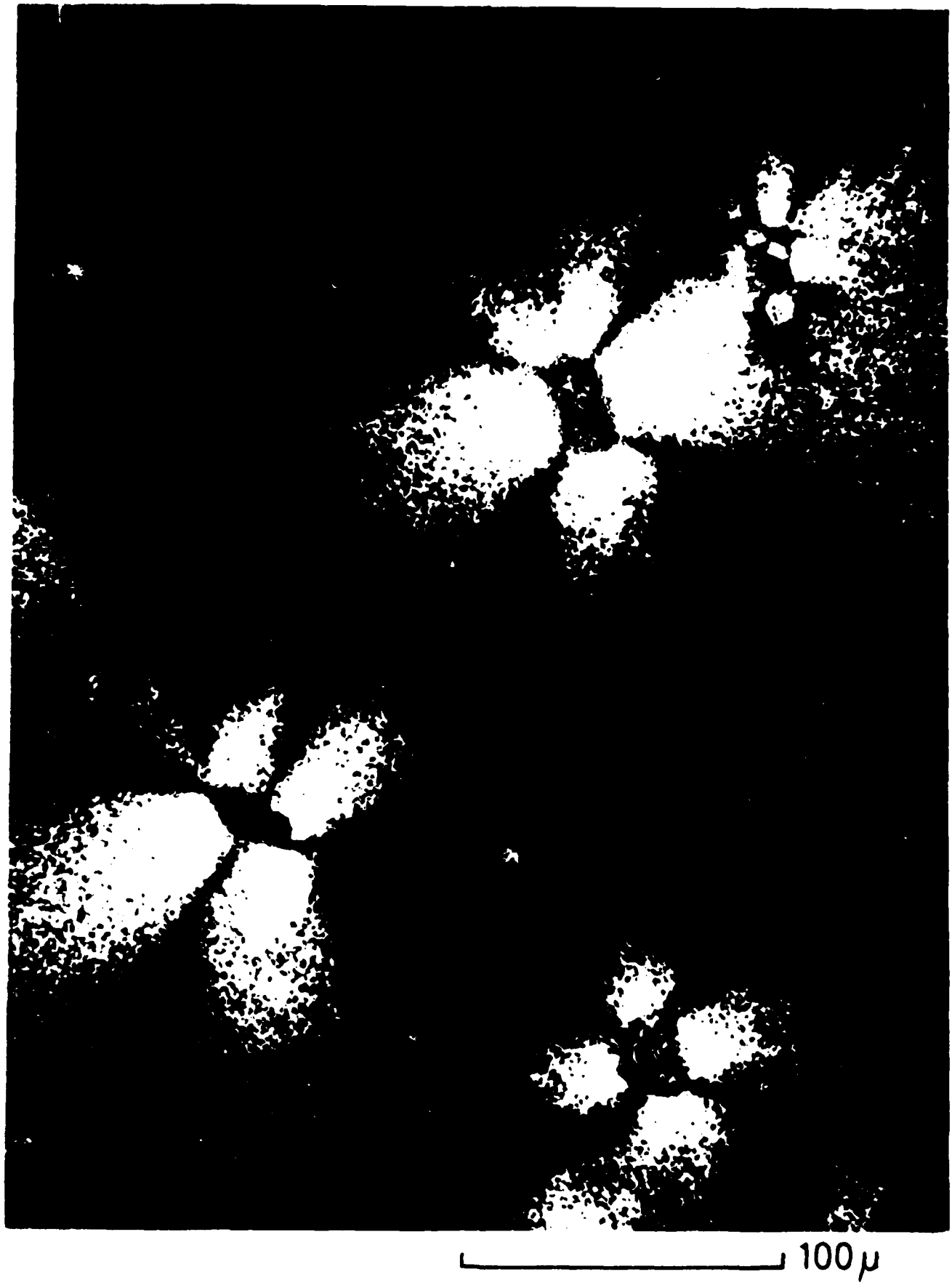

Figure 12. Photoelastic image of pressure pockets located within the adhesive after 48 hours immersion in distilled water at 60C.

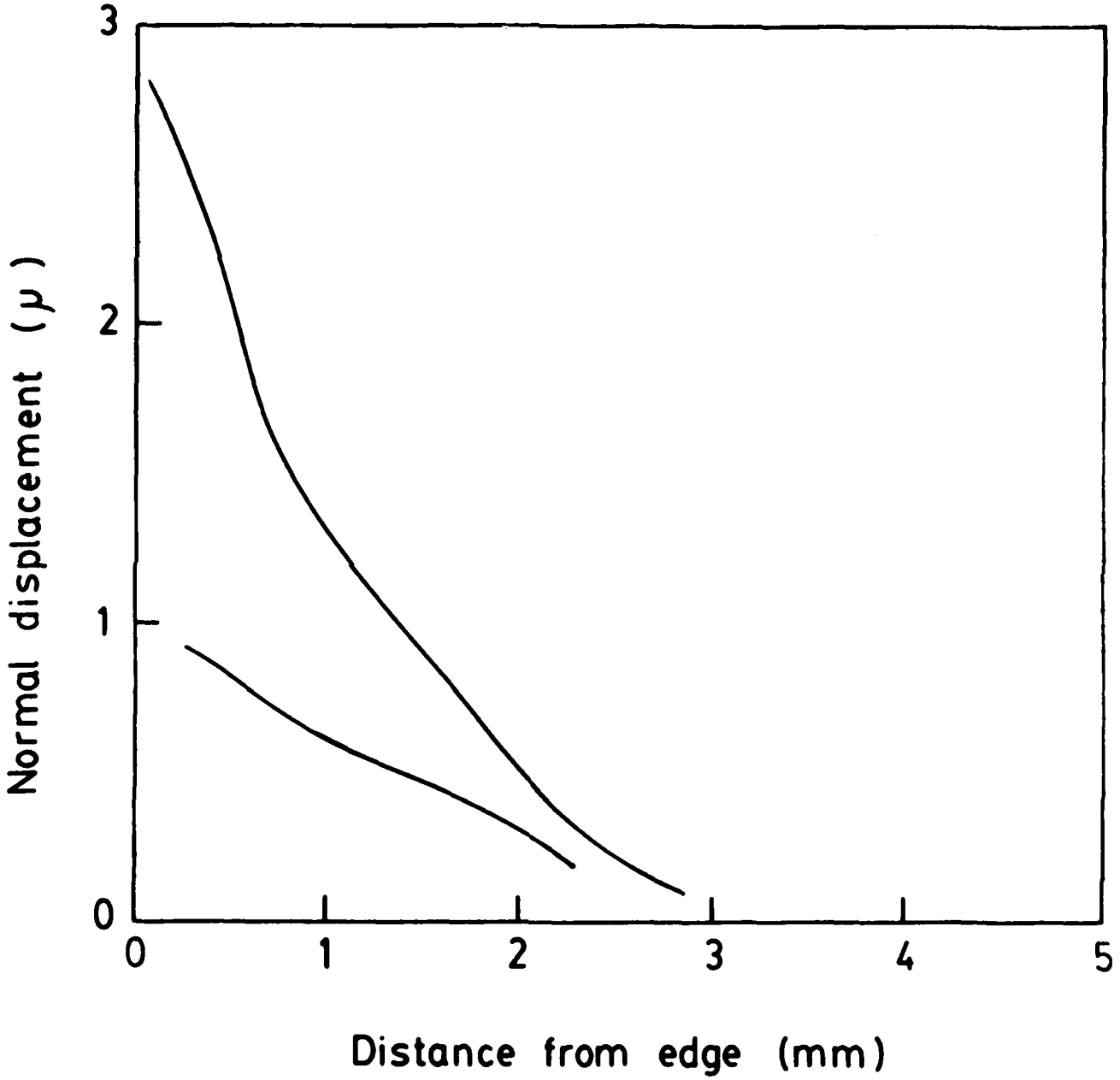

Figure 13. Radial distribution of displacement of the cover slip normal to a Redux 312/5 joint after 120 hours immersion at 60C.
Upper curve; cover slip/Redux 312-5/glass, distilled water
Lower curve; cover slip/Redux 312-5/glass, saturated NaCl solution

a

b

Figure 14. An E-glass/polyester resin composite after 3 days immersion in boiling water. (a) Viewed with transmitted light. (b) Same as (a) but with polars crossed. The action of diffused water at the interface has destroyed the transfer of load arising from resin shrinkage, thereby rendering the fibres stress-free and therefore

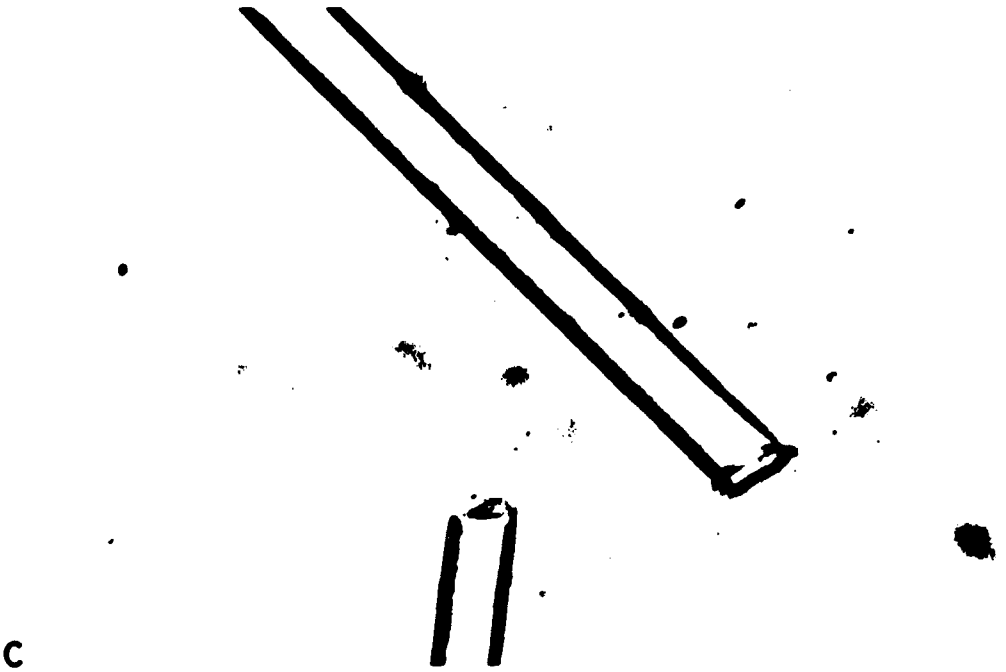

c

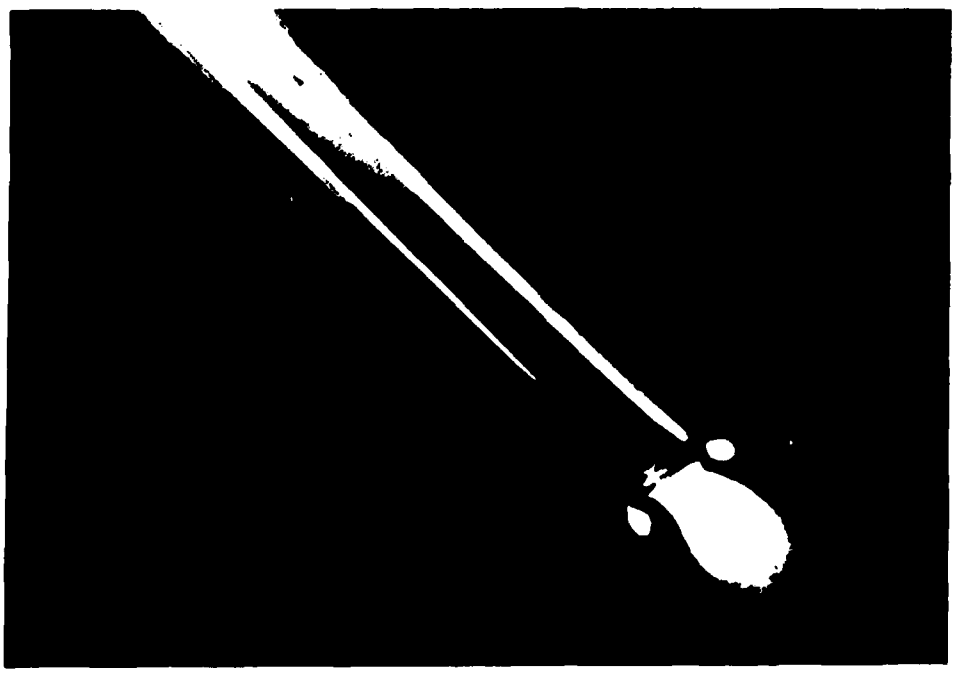

d

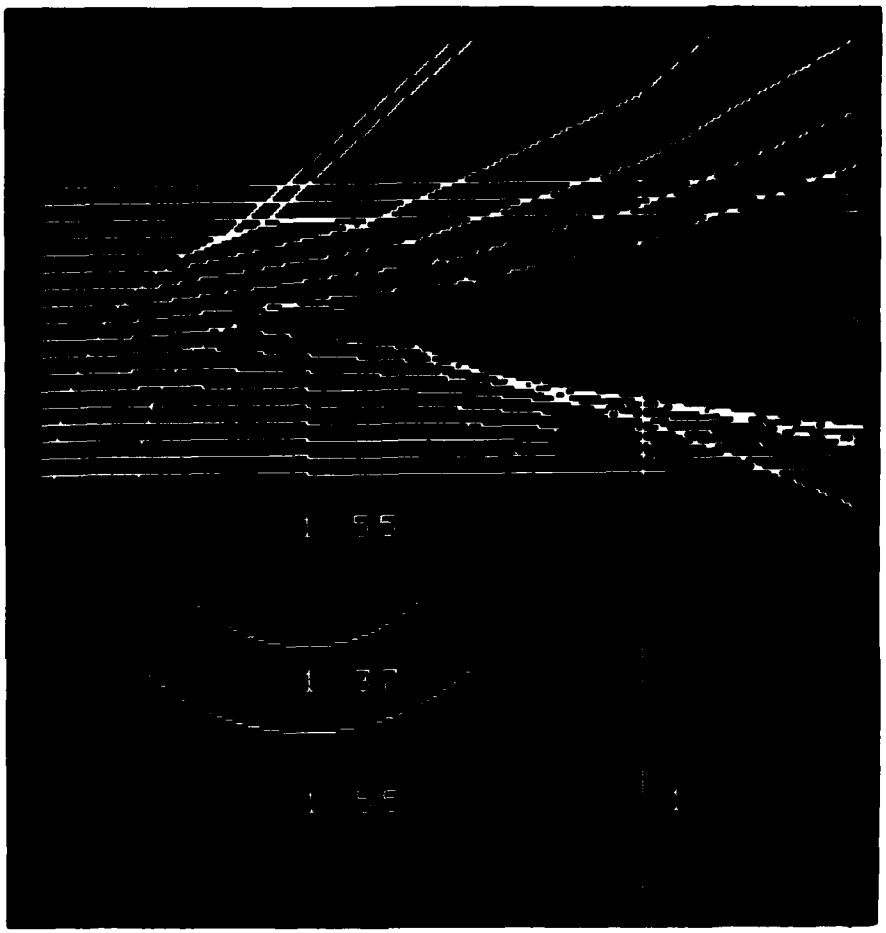

a

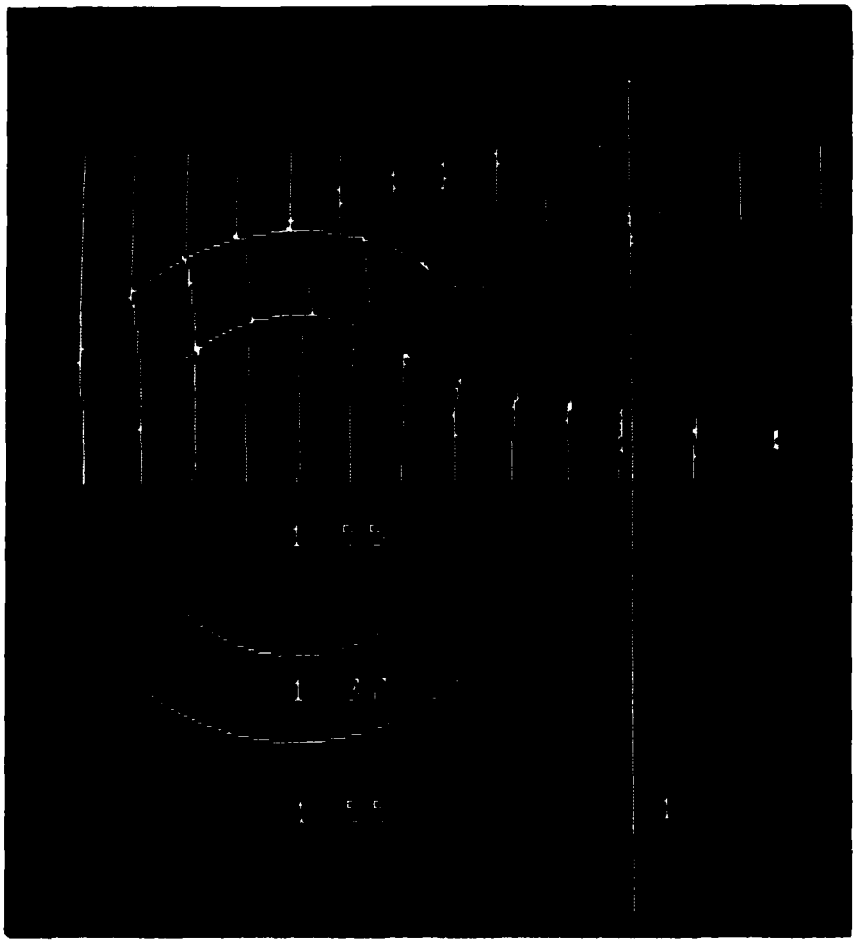

b

Figure 15a.Ray diagram reconstruction for a glass fibre embedded in resin with a water solution at the interface. Fibre diameter is 10μm. Interfacial gap is ~ 1/2 a fibre diameter.

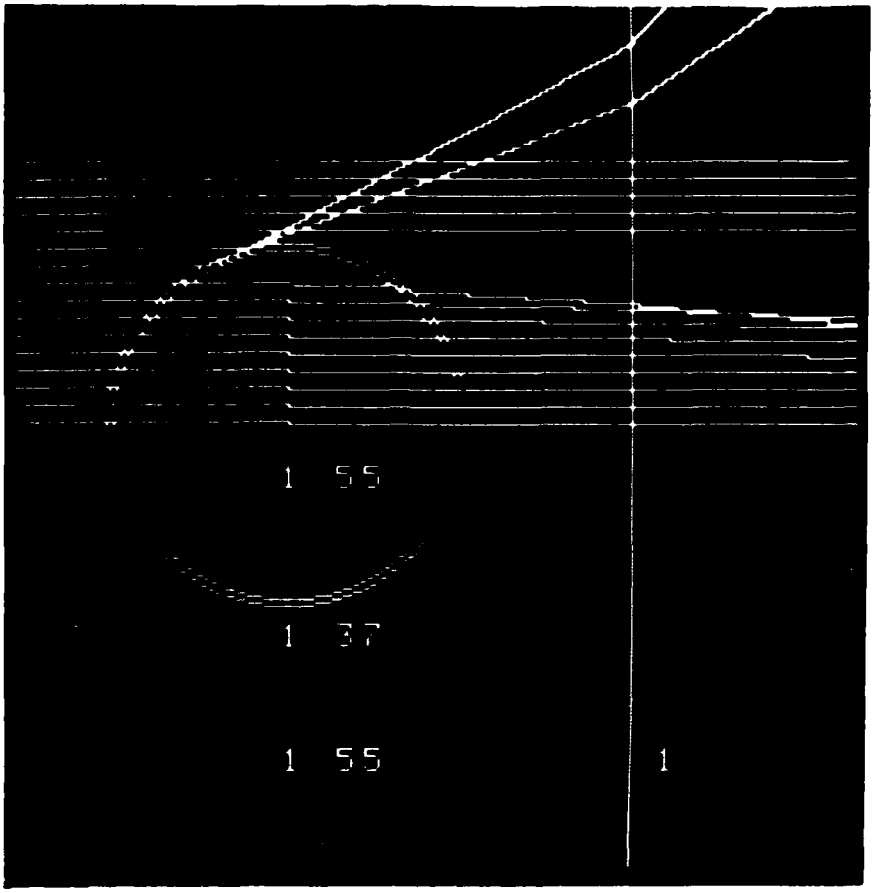

a

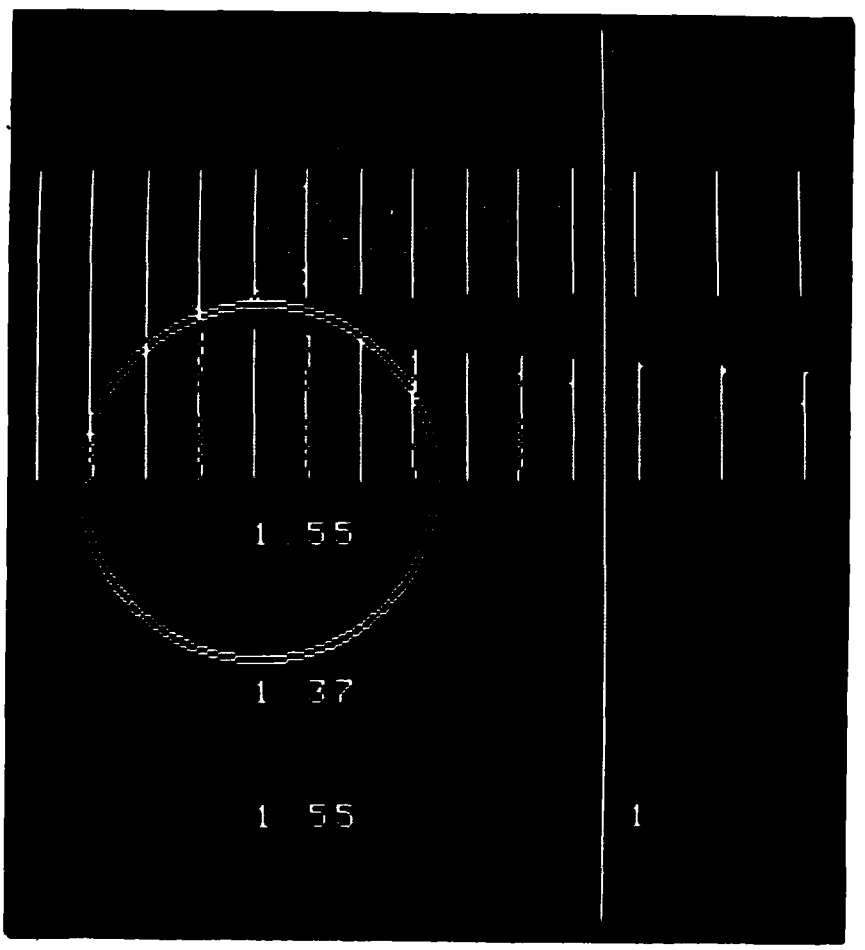

b

Figure 16a.Ray diagram reconstruction for a glass fibre embedded in resin with a water solution at the interface. Fibre diameter is 10μm. Interfacial gap is λ/2.

b.Same as (a) but showing the wavefronts. Wavefronts plotted at 4λ

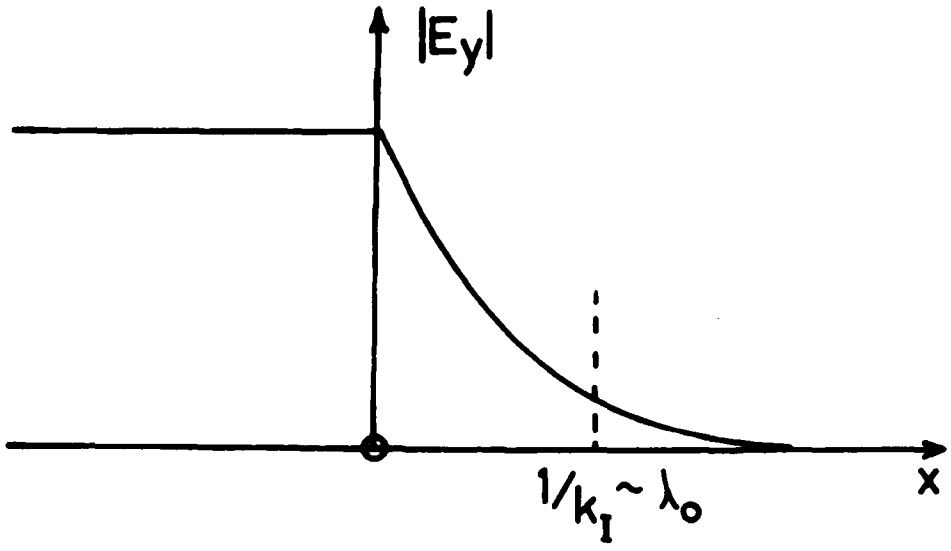

Figure 17. Graph showing the "transmitted" electric field amplitude as a function of distance from the interface following total internal reflection. After Feynman[25].

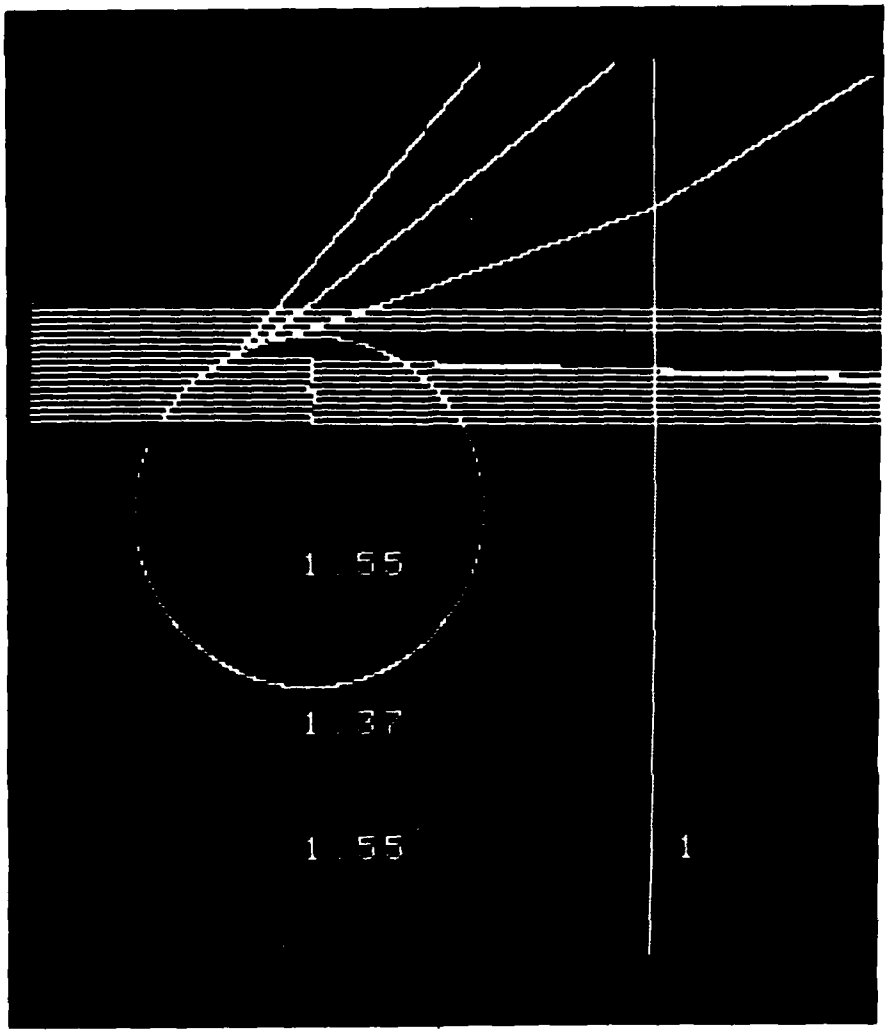

Figure 18. Ray diagram reconstruction for a glass fibre embedded in resin with a water solution gap of λ/20. Ignoring the consequences of the "transmitted flux".

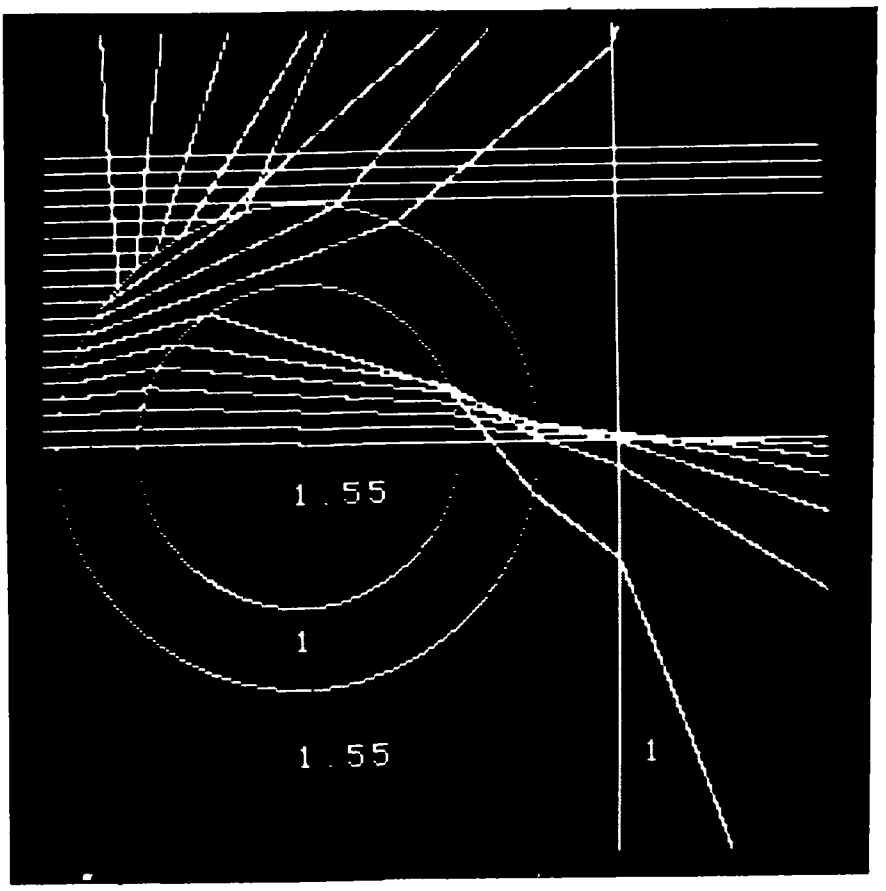

a

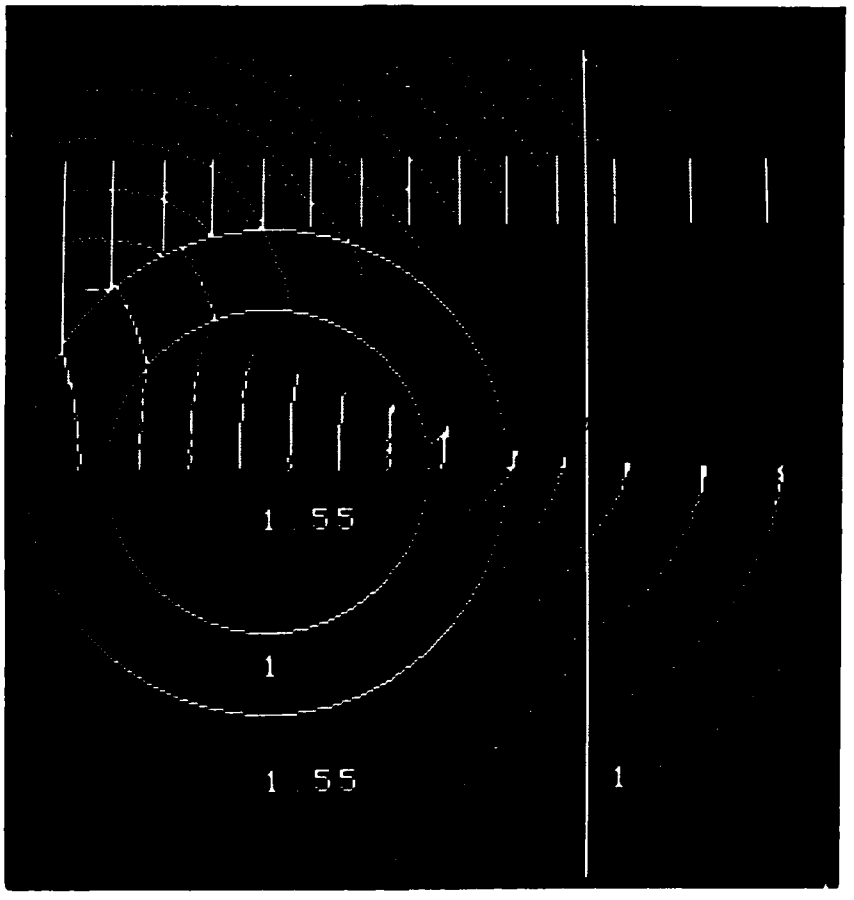

b

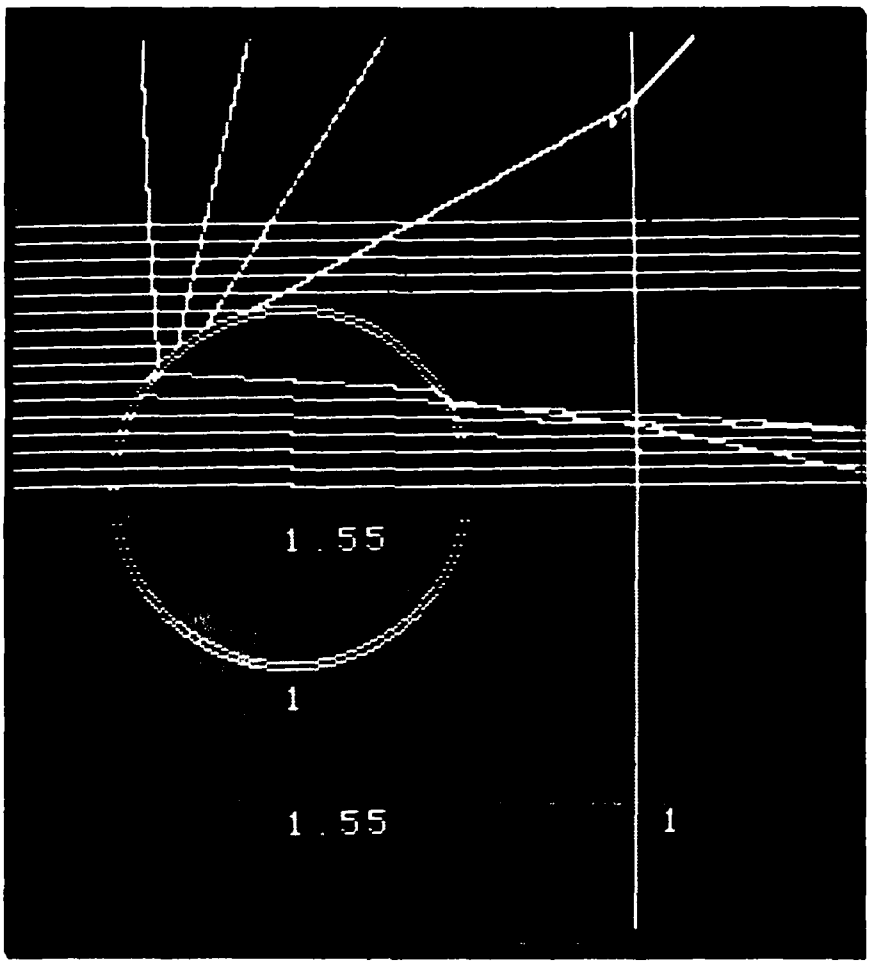

a

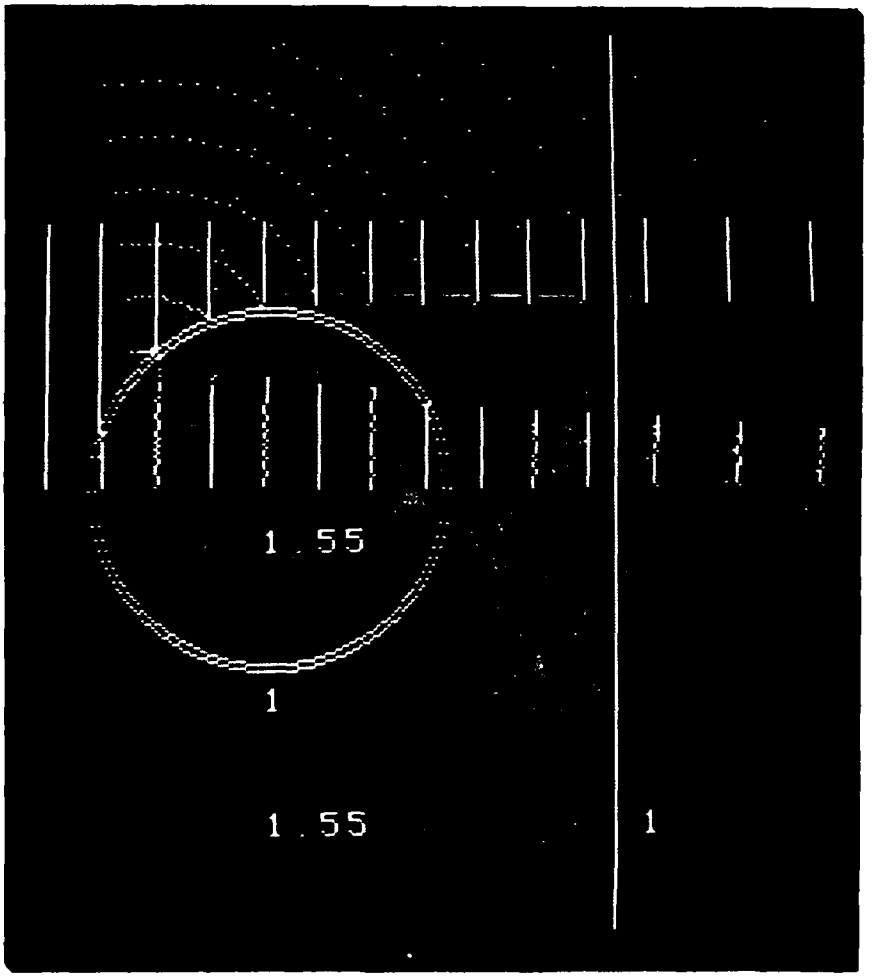

b

a

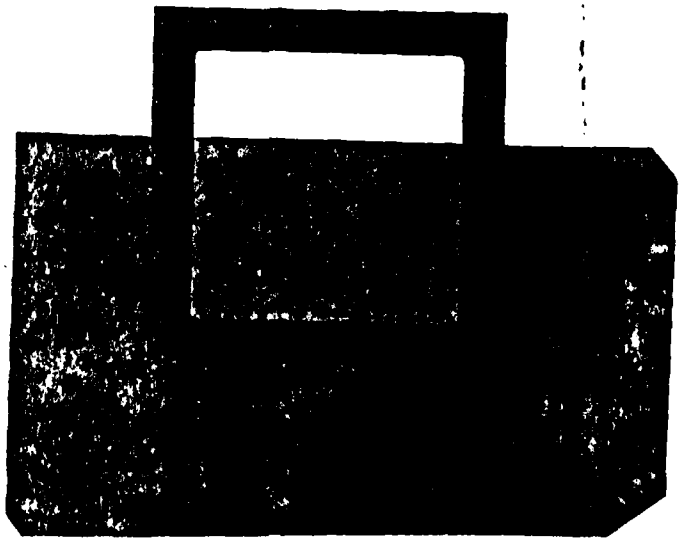

b

Fgure 21. Frosted glass slide viewed (a) with uncrossed and (b) with crossed polars.